An analytical model of an elementary elliptical cell forming an alveolar elastic material under plane stress

Gourinat, Yves and Belloeil, Victorien

Abstract

This paper analyzes the static behavior of alveoled materials that is about to be developed for dynamic optimization of structural panels. It deals precisely with materials made of elliptical thin cells, filled with polymer material. The main contribution of the paperconsists in elaborating an analytical approach describing the material. The considered problem represents an unidirectional stress, the goal being to calculate the elastic energy and strain globally obtained in the material. The wall of the elementary cell is represented in accordance with the classical BRESSE's theory of thin beams, with specific adaptation for elliptical shape. The polymer material filling the cell is modelized with ABSI's method of equivalence, which allows a direct approximation of various continuous media by equivalent spring segments. This method is presented and discussed for the present configuration, with its specific adaptation. The final result obtained by these analytical approaches is then compared to results from a finite element model. In spite of local differences between the analytical results and numerical computation, it appears clearly that the precision obtained by the proposed analytical approach is better than 95%, which is sufficient for this kind of material. Thus, the proposed analytical calculation and methodology allows robust and quick determination of material characteristics for elementary cells of such alveoled materials. The resulting laws can then be introduced into global models of a grid of cells.

1. Introduction

The goal of this paper is to propose an analytical modeling of alveoled material, considering the rigidity of an elementary cell. In fact, the material is composed of joined elliptical beams filled with an elastic material.This assembly is submitted to membrane stress, in order to analyze its stiffness.

The originality of the approach consists in combining classical elastic methods for each component, in order to define a global behavior which can be implemented in a general model of such structural elements.

The elliptical ring is calculated under Bresse's assumptions,with integration of thin beam theory, and the elastic filling material is modeled through ABSI's equivalence [1], representing orthogonal rigidities of the mesh, the stiffness being deduced from an energetic approach of strains. This kind of method, in the frame of MENABREA's theorem, is finally used to determine the resulting deformation of the complete cell. Finite element modeling is used to validate each step of the methodology, and is presented in this paper. The final characteristics of the cell may eventually be used to
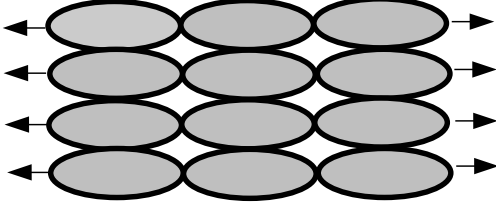
Fig. 1. Alveoled material.

create a specific alveolar type which could possibly be added to the available package of elements.

The approach presented in this paper is inspired by the ring approach [2–6]. This analytical solution measures the deflection of a circular sprig under stress, and also [7] presents an analytical solution of elliptic arches. The material studied in this article is a cellular material, which can be studied by [8] under uniaxial strength (see Fig. 1).

2. Analytical method

A schematic diagram of a ring is modeled in Fig. 2(a). The ring is subjected to unidirectional load *F* in direction **y**. Deformations of the ring are calculated with BRESSE's formulas. The ellipse deformation uses a modification of BRESSE's formulas for an elliptical curved beam.

BRESSE's formulas are applied to a curved beam in small displacement, and enable the calculation of the rotation and the displacement of a point *A* when the dis-

placement and the rotation of point *B* (another point of the curved beam) are known. These formulas are given by LAROZE [9]. The first equation of BRESSE:

$$\vec{\omega_2} = \vec{\omega_1} + \int_{s_1}^{s_2} \left(\frac{\vec{M_y}}{EI_y} + \frac{\vec{M_z}}{EI_z} + \frac{\vec{M^t}}{GJ} \right) ds$$

The second equation of BRESSE:

$$\vec{\Lambda_1} = \vec{\Lambda_2} + \vec{\omega_1} \times \overrightarrow{G_1G_2} + \int_{s_1}^{s_2} \left(\frac{\vec{N}}{ES} + \kappa_y \frac{\vec{T_y}}{GS} + \kappa_z \frac{\vec{T_z}}{GS} \right) ds$$
$$+ \int_{s_1}^{s_2} \left(\left[\frac{\vec{M_y}}{EI_y} + \frac{\vec{M_z}}{EI_z} \right] \times \overrightarrow{GG_2} + \frac{\vec{M^t}}{GJ} \times \overrightarrow{CG_2} \right) ds$$

where $\vec{\omega_i}$ is the rotation vector of point i, $\vec{\Lambda_i}$ its translation vector, and $\times$ is the vector cross product.

A finite elements model is created with the commercial code SAMCEF. This model is used to validate the theoretical model. The comparison between the two models is realized with 10 cases.

2.1. Theoretical background

2.1.1. Ring approach

Consider a ring subjected to two equal and diametrically opposed radial tensile forces *F*, see Fig. 2(a). The ring radius is *R*, and the center point is *O*.

In this 2*D* problem, three parameters are present N, T_y and M_z. This problem has one symmetric at axis $(x'Ox)$, so T parameter is equal to zero at the point *A* and *C*. One can also note the symmetry axis $(y'Oy)$
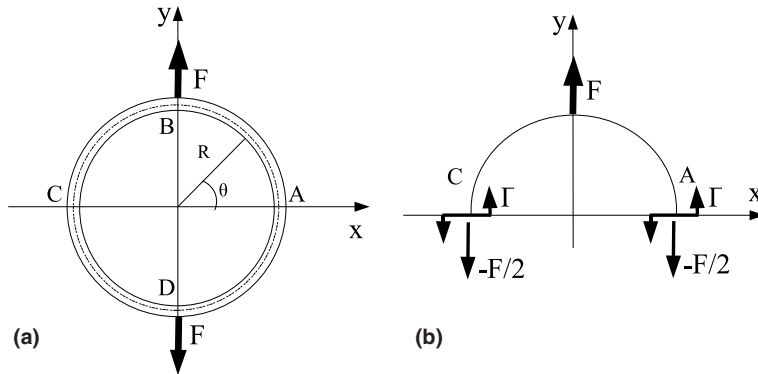

Fig. 2. (a) Circle with a constant load. (b) Reduced loading system of a semi-circular ring subject to a diametrical load *F*.

consequently the bending moment of both point A and C are equal, with Γ the bending moment.

This approach can be divide into two sections as shown in Fig. 2(b).

Section one $[AB]$ $(0 < \theta < \pi/2)$

$$\left[\begin{array}{rcl} N & = & \frac{F}{2}\cos(\theta), \\ T & = & -\frac{F}{2}\sin(\theta), \\ M & = & \frac{FR}{2}(1 - \cos(\theta)) + \Gamma \end{array}\right.$$

Section two $[BC]$ $(\pi/2 < \theta < \pi)$

$$\left[\begin{array}{rcl} N & = & -\frac{F}{2}\cos(\theta), \\ T & = & \frac{F}{2}\sin(\theta), \\ M & = & \frac{FR}{2}(1 + \cos(\theta)) + \Gamma. \end{array}\right.$$

Considering the symmetry at points A and C, the sections S_A and S_B do not turn in the deformation, so the first BRESSE's equation is given by Eq. (1). And this equation has only one unknown value Γ.

$$\int_0^{\pi/2} M\,d\theta = 0$$

i.e., $\displaystyle\int_0^{\pi/2} \left[\frac{FR}{2}(1 - \cos(\theta)) + \Gamma\right] d\theta = 0.$ \hfill (1)

So, $\Gamma = -0.1817 FR$.

The second equation of BRESSE gives the displacement at points A and B.

$$u_A = -0.068\frac{R^3 F}{EI} + 0.25\left(\frac{1}{E} - \frac{\kappa}{G}\right)\frac{RF}{S},$$

$$v_B = 0.074\frac{R^3 F}{EI} + 0.393\left(\frac{1}{E} + \frac{\kappa}{G}\right)\frac{RF}{S}, \hfill (2)$$

where $\psi = \theta + \pi/2$, $\quad x = R\cos\theta$, $\quad y = R\sin\theta \quad$ and $\kappa = \frac{8v^2 + 14v + 7}{6(1+v)^2}$.

2.1.2. Ellipse approach

Determination of displacement at the point with an elliptic geometry is an improvement of BRESSE's meth-

od. The ellipse is subject to diametrical load F, see Fig. 3(a), a the short axis and b the long axis.

The elliptical loop equation is defined by the following Eq. (3).

$$\begin{cases} x = a\cos t, \\ y = b\sin t. \end{cases} \hfill (3)$$

The curvilinear parameter is

$$ds = \sqrt{a^2\sin^2 t + b^2\cos^2 t}\,dt. \hfill (4)$$

The BRESSE's equations are modified in these configurations, and in view of symmetry (see Fig. 3(b)), only one quadrant can be considered as an originally straight strut $[AB]$, where $t \in [0; 2\pi]$.

$$\left[\begin{array}{rcl} N & = & \frac{F}{2}\frac{b\cos t}{\sqrt{a^2\sin^2 t + b^2\cos^2 t}}, \\ T & = & \frac{F}{2}\frac{-a\sin t}{\sqrt{a^2\sin^2 t + b^2\cos^2 t}}, \\ M & = & \frac{Fa}{2}(-1 + \cos t) + \Gamma. \end{array}\right.$$

Considering the same consideration that the Eq. (1) Γ is determined by the first equation of BRESSE. And the displacements are defined by the Eq. (5).

$$\begin{aligned} u_A &= \int_{S_A}^{S_B} \frac{N\cos\psi}{ES} - \frac{\kappa T\sin\psi}{GS} - (y_A - y)\frac{M}{EI}\,ds \\ &= \int_{S_A}^{S_B} \frac{N\cos\psi}{ES} - \frac{\kappa T\sin\psi}{GS} + y\frac{M}{EI}\,ds \\ &= \int_0^{\pi/2} \left[\frac{N\sin t}{ES} + \frac{\kappa T\cos t}{GS} + y\frac{M}{EI}\right]ds, \end{aligned}$$

$$\begin{aligned} v_B &= \int_{S_A}^{S_B} \frac{N\sin\psi}{ES} + \frac{\kappa T\cos\psi}{GS} + (x_A - x)\frac{M}{EI}\,ds \\ &= \int_{S_A}^{S_B} \frac{N\sin\psi}{ES} + \frac{\kappa T\cos\psi}{GS} - x\frac{M}{EI}\,ds \\ &= \int_0^{\pi/2} \left[\frac{-N\cos t}{ES} + \frac{\kappa T\sin t}{GS} - x\frac{M}{EI}\right]ds. \end{aligned} \hfill (5)$$

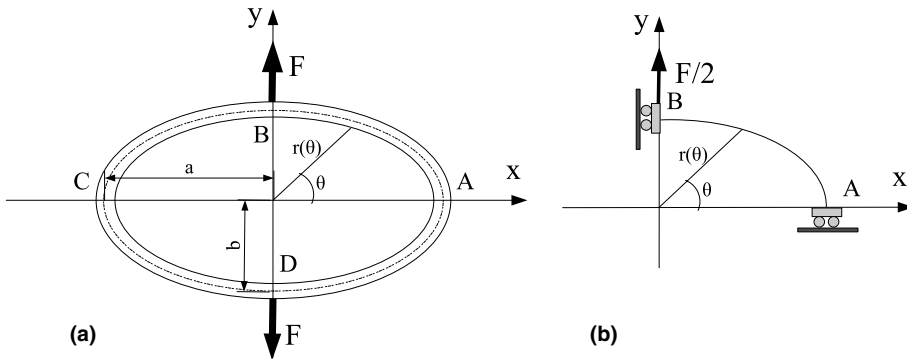These displacements of point A and B are calculated by MATLAB script, with symbolic integration. The

Fig. 3. (a) Ellipse with a constant load. (b) Reduced loading system of an ellipse subject to a diametrical load F.

MATLAB script first calculates in the value of Γ, and next the analytical values of N, T, and M are replaced in the Eq. (5), and the integration on $[0;\pi/2]$ gives the value of u_A and v_B.

This program also calculates the strain energy (Eq. (6)).

$$E_{\text{def}} = \frac{1}{2} \int_{s_1}^{s_2} \left(\frac{N^2}{ES} + \frac{M^2}{EI} + \frac{\kappa T^2}{GS} \right) \mathrm{d}s \qquad (6)$$

2.2. Validation of model

2.2.1. Numerical analysis

To validate the theoretical model, a comparison with a finite elements model is presented below for various configurations, and is studied using a commercial code SAMCEF.

The finite elements model deformations are calculated with the linear module ASEF. The full model is considered in this study. All models are meshed with beam elements (.BEAM command in SAMCEF), and the load is applied on the diametrically opposed nodes. There are 200 elements and 401 nodes, and material property is shown in Table 1.

Fig. 4 shows the definition of the section and the different parameters of the ellipse. The configuration studied is an ellipse with a long axis a and a short axis b. The cross section has a thickness H and a width B. The applied load at the points B and D is equal to $-1000N$ for the full model.

In all cases, three configurations are studied ellipse case, ring case, and numerical case. For the ring case, the ring radius is $R = \frac{a+b}{2}$. These configurations can enable validation of the analytical model with two other models. The numerical model allows the validation for all cases. The ring case allow the validation of the numerical case and the ellipse case for circular configuration.

Table 1
Material property

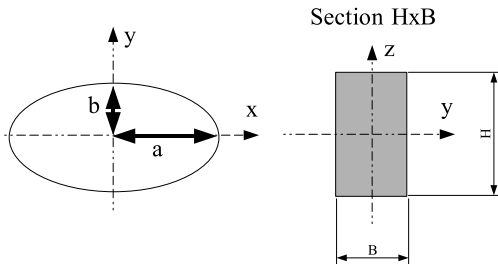|	Polyetherimide (PEI)
Elastic modulus (Pa)	3.1×10^{10}
Poisson's ratio	0.36

Section HxB

Fig. 4. Geometry of ellipse.

2.2.2. Results and discussion

Variations of models are summarized in Table 2. Figs. 5 and 6 show the evolution of the relative error[1].

In the ellipse model, it can be clearly observed in Fig. 5 a maximal relative error of 4.5%. The finite elements model shows a good agreement with the theoretical model. The theoretical model is a good approximation of ellipse deformation.

The relative error for the ring model, see Fig. 6, has good results in circular configuration. The maximal error relative in these cases is less than 1% against the finite elements model, and less than 1% against the ellipse model. Nevertheless this model has results more moved away of numerical deformation.

Table 6 gives the value of the rate of damping of the ellipse under uniaxial stress. For a short fixed axis, the rate increases with the rise of the long axis a.

3. Discrete method

In this part, an ellipse is filled with an elastic material, see Fig. 7. This model is subject to a uniaxial stress.

The BRESSE's formulas can be used with a curved beam, but a different method is required for elastic-filled ellipse.

A discrete method is used. The ellipse is made up of eight springs. The elastic material is modeled with ABSI's theory [1], which divides the plate on a trellis of beams. The trellis is modeled with springs. Hence, an ellipse filled with an elastic material can be modeled with a trellis of springs.

An energetic method [10] is used to calculate the deformation of the ellipse. This method is MENEBREA's theory, in which the strain energy is determined and a minimization is used to compute the values of the displacement at the nodes.

3.1. Single ellipse

The single ellipse is made up of four springs and four angular springs, see Fig. 8. The ellipses studied have loads F applied at points B and D.

The potential energy of this model is

$$
\begin{aligned}
EPT = {} & \frac{C}{4}(\theta^A - \theta_0^A)^2 + \frac{C}{4}(\theta^C - \theta_0^C)^2 + \frac{C}{4}(\theta^B - \theta_0^B)^2 \\
& + \frac{C}{4}(\theta^D - \theta_0^D)^2 + \frac{k}{2}(L_{AB} - L_{AB}^0)^2 \\
& + \frac{k}{2}(L_{BC} - L_{BC}^0)^2 + \frac{k}{2}(L_{CD} - L_{CD}^0)^2 \\
& + \frac{k}{2}(L_{DA} - L_{DA}^0)^2 - Fv_D - Fv_B \qquad (7)
\end{aligned}
$$

---

[1] The relative error is $\%\text{error} = \frac{w_u - w_o}{w_o}$, where w_o is the displacement of the finite element model.

Table 2
Displacement results (in mm)

| Cases		1	2	3	4	5	6	7	8	9	10
a		10	20	30	30	10	20	30	30	30	10
b		20	20	20	20	30	30	30	40	40	50
H		8	8	8	8	8	8	8	8	8	8
B		5	5	5	8	5	5	5	5	8	5
SAMCEF	u_a	8.20×10^{-2}	2.21×10^{-1}	4.01×10^{-1}	1.02×10^{-1}	1.52×10^{-1}	4.01×10^{-1}	7.28×10^{-1}	1.12×10^{0}	2.79×10^{-1}	3.53×10^{-1}
	$-v_b$	5.39×10^{-2}	2.57×10^{-1}	7.06×10^{-1}	1.87×10^{-1}	6.51×10^{-2}	3.00×10^{-1}	8.18×10^{-1}	9.15×10^{-1}	2.39×10^{-1}	8.82×10^{-2}
	v_b/u_a	0.66	1.16	1.76	1.83	0.42	0.75	1.12	0.82	0.86	0.25
Ring	u_a	$9.50\ 10^{-2}$	2.20×10^{-1}	4.22×10^{-1}	1.07×10^{-1}	2.20×10^{-1}	4.22×10^{-1}	7.24×10^{-1}	1.14×10^{0}	2.85×10^{-1}	7.24×10^{-1}
	$-v_b$	1.17×10^{-1}	2.56×10^{-1}	4.81×10^{-1}	1.30×10^{-1}	2.56×10^{-1}	4.81×10^{-1}	8.13×10^{-1}	1.28×10^{0}	3.29×10^{-1}	8.13×10^{-1}
	v_b/u_a	1.23	1.16	1.14	1.21	1.16	1.14	1.12	1.12	1.15	1.12
Ellipse	u_a	7.84×10^{-2}	2.20×10^{-1}	4.06×10^{-1}	1.05×10^{-1}	1.45×10^{-1}	3.97×10^{-1}	7.27×10^{-1}	1.11×10^{0}	2.76×10^{-1}	3.42×10^{-1}
	$-v_b$	5.40×10^{-2}	2.57×10^{-1}	7.03×10^{-1}	1.86×10^{-1}	6.64×10^{-2}	3.01×10^{-1}	8.17×10^{-1}	9.16×10^{-1}	2.40×10^{-1}	8.94×10^{-2}
	v_b/u_a	0.68	1.16	1.73	1.77	0.46	0.76	1.12	0.83	0.87	0.26
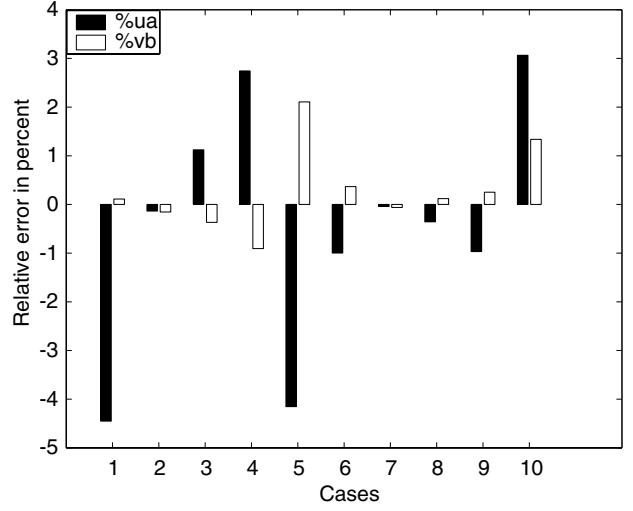
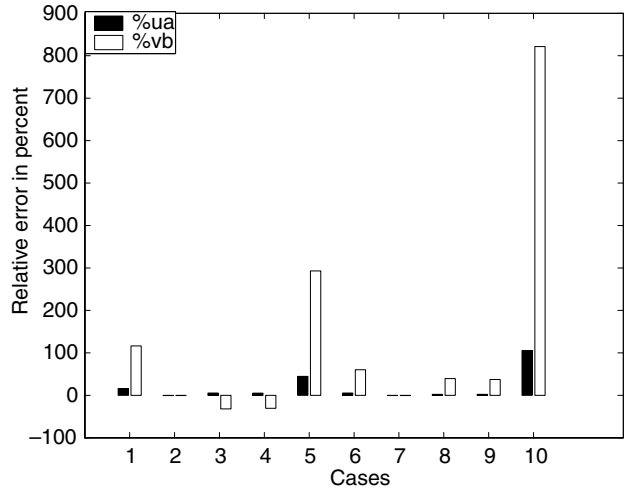Fig. 5. Evolution of ellipse relative error.

Fig. 6. Evolution of ring relative error.

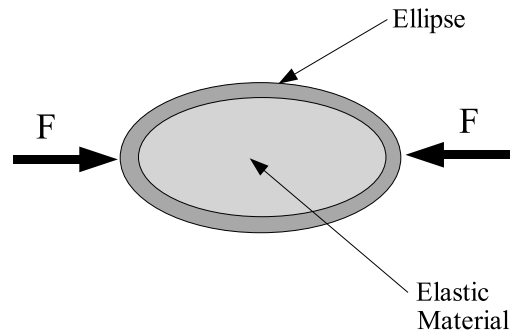Fig. 7. Schematic ellipse with elastic material.

where k is an equivalent rigidity of a beam, during a tensile test, $k = \frac{ES}{l}$.

An energetic method is used, but the angular spring (C) is an undefined constant. So the theoretical model (the ellipse model) is used to recover the deformation, and the potential energy.
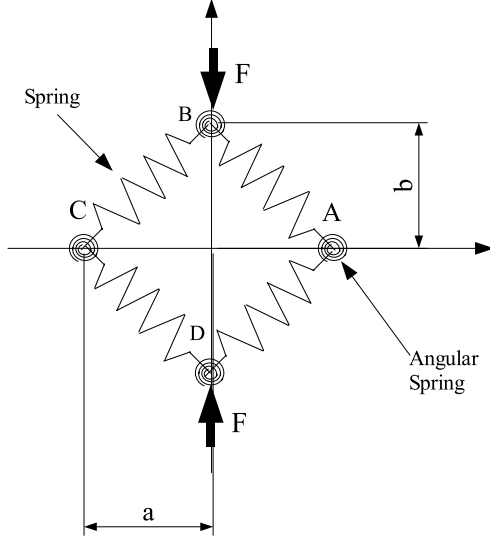
Fig. 8. Discrete model.

Fig. 9. Schema of the bar [AB].

Fig. 10. Schematic clamped bar.

An identification between these models gives the value of the C parameter. All parameters of the discrete model are defined and can be used in the next stages of calculation.

3.2. Ellipse filled with elastic material

3.2.1. ABSI's theory

ABSI's theory allows the transformation of plates into a trellis of beams. The condition of equivalence between the real body and the fictive body (trellis of beams) is the equality of strain energies.

Consider a real body with an applied load, where u_k is the displacement on the $\mathbf{x}_k$ axis (x_1, x_2, x_3). The strain tensor is

$$e_{ij} = \frac{1}{2}\left(\frac{\partial u_i}{\partial x_j} + \frac{\partial u_j}{\partial x_i}\right).$$

The strain density U_o is given by

$$U_o = \frac{1}{2}\lambda(e_{ii})^2 + \mu e_{ij}e_{ij}. \tag{8}$$

Consider a bar [AB], with a length of l, and with a normal stress N. So the relation, which relates uniaxial stress and strain, is

$$N = ES\frac{\Delta l}{l} = ES\varepsilon,$$

where S is the beam section, ε the unit strain. The strain energy W' is

$$W' = \frac{1}{2}N\Delta = \frac{1}{2}ESl\varepsilon^2 = \frac{1}{2}\rho\varepsilon^2.$$

The bar [AB] is schematized in Fig. 9. The unit strain ε of the bar is described by

$$\varepsilon = \frac{\partial u'_1}{\partial x'_1} = \alpha_i\frac{\partial u_i}{\partial x_i}\frac{\partial u_j}{\partial x_j} = \alpha_i\alpha_j\frac{\partial u_j}{\partial x_j} = \alpha_i\alpha_j e_{ij},$$
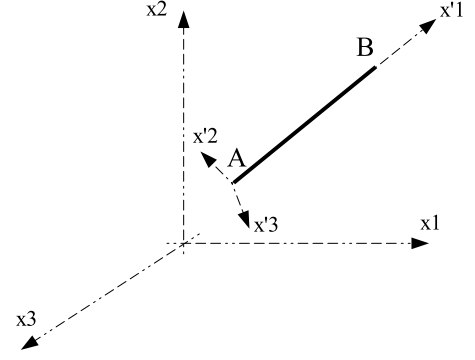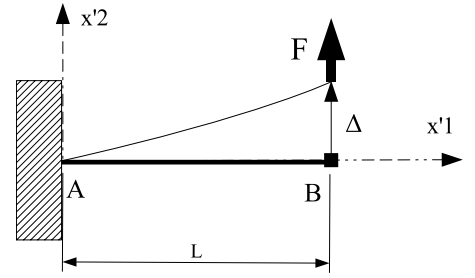
where α_i is the cosine director of x'_1, $u'_1 = \alpha_i u_i$. Pointing out β_i the sine director of x'_2, an other equation is given by

$$\frac{\partial u'_2}{\partial x'_1} = \beta_i\alpha_j\frac{\partial u_i}{\partial x_j}.$$

The strain deformation is described by

$$W' = \frac{1}{2}N\varepsilon l = \frac{1}{2}ESl\varepsilon^2 = \frac{1}{2}\rho\varepsilon^2 = \frac{1}{2}\rho(\alpha_i\alpha_j e_{ij})^2. \tag{9}$$

The geometry of the bar is modified, point A is clamped, and a load is applied at point B (Fig. 10). The deflection Δ is related to the applied load F by

$$F = \frac{3EI}{l^3}\Delta. \tag{10}$$

So the strain energy W'' is given by

$$W'' = \frac{1}{2}F\Delta = \frac{3}{2}\frac{EI}{l}\left(\frac{\Delta}{l}\right)^2 = \frac{1}{2}\eta\left(\frac{\Delta}{l}\right)^2.$$

The geometry is modified with adding a rotation θ on the bar, see Fig. 11. So the deflection BB' is equal to

$$BB' = \frac{\partial u'_2}{\partial x'_2}l = \Delta + \theta l = \alpha_j\beta_i\frac{\partial u_i}{\partial x_j}.$$

The strain energy is described by Eq. (11)

$$W'' = \frac{1}{2}\eta\left(\alpha_j\beta_i\frac{\partial u_i}{\partial x_j} - \theta\right)^2. \tag{11}$$

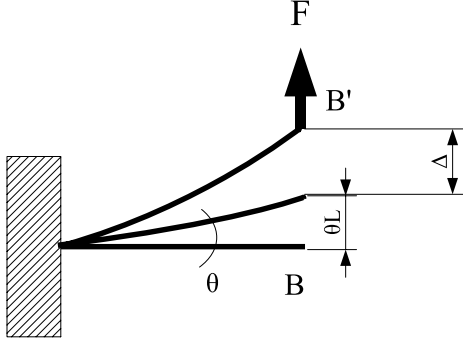So the total energy of bar [AB] is the sum of Eqs. (9) and (11)

$$W_{AB} = W' + W''$$

Fig. 11. Schematic clamped bar with a rotation.

3.2.2. Application of ABSI's theory

Consider the strain on axis $\mathbf{x}_3$ ($e_{i3} = 0$), so the strain density is

$$U_o = \frac{1}{2}\lambda(e_{11} + e_{22})^2 + \mu\Big[(e_{11})^2 + (e_{22})^2 + 2(e_{12})^2\Big].$$

The problem is studied in planar strain condition. In order to include this model in the discrete model ([1]), the elastic material is a rhomb, Fig. 12. This model consists of bars and a rigid body (point H).

The bars in the outline of rhomb only work under normal stress. Their strain energies are given by the Eqs. (12) and (13). On the bars $[AD]$ and $[BC]$ the cosine directors are $\alpha_1 = \cos\alpha$ and $\alpha_2 = \sin\alpha$ and the sine directors are $\beta_1 = -\sin\alpha$ and $\beta_2 = \cos\alpha$. So

$$W'_{AD} = W'_{BC}$$
$$W'_{AD} = \frac{1}{2}\rho_{AD}[e_{11}\cos^2\alpha + e_{22}\sin^2\alpha + 2e_{12}\sin\alpha\cos\alpha]^2.$$

(12)

For bars $[DB]$ and $[AC]$, the strain energy is given by

$$W'_{CA} = W'_{BD}$$
$$W'_{CA} = \frac{1}{2}\rho_{AC}[e_{11}\cos^2\alpha + e_{22}\sin^2\alpha + 2e_{12}\sin\alpha\cos\alpha]^2.$$

(13)

The diagonal bars work in flexion, so their energies in compression are given by the following Eq. (14).
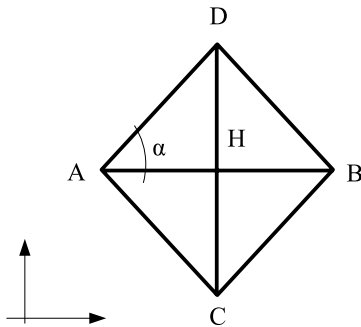

Fig. 12. ABSI's rhomb.

$$\begin{cases} W'_{HA} = W'_{HB} = \frac{1}{2}\rho_{HA}(e_{11})^2 \\ W'_{HC} = W'_{HD} = \frac{1}{2}\rho_{HC}(e_{22})^2 \end{cases}$$

(14)

and Eq. (15) gives their energies in flexion

$$\begin{cases} W''_{HA} = W''_{HB} = 2\eta_{HB}\left(\frac{\eta_{HD}}{\eta_{HD}+\eta_{HB}}\right)^2(e_{12})^2, \\ W''_{HC} = W''_{HD} = 2\eta_{HD}\left(\frac{\eta_{HB}}{\eta_{HD}+\eta_{HB}}\right)^2(e_{12})^2. \end{cases}$$

(15)

The equality of strain energy W gives

$$W = AU_o,$$
$$W = 2W'_{AD} + 2W'_{AC} + 2W'_{HB} + 2W'_{HD} + 2W''_{HB} + 2W''_{HD}.$$

(16)

The energy U_o is given by Eq. (8), and the others energies are equal to Eqs. (12)–(15).The identification between these equations gives the value of the constant parameter ρ.

$$\begin{cases} \rho_{AD} = \frac{\lambda A}{4\sin^2\alpha\cos^2\alpha}, \\ \rho_{HA} = \frac{4}{2}(\lambda + 2\mu - \lambda\cot g^2\alpha), \\ \rho_{HD} = \frac{4}{2}(\lambda + 2\mu - \lambda tg^2\alpha). \end{cases}$$

(17)

So the ABSI's model can be added to the discrete model, and the new model is schematized on Fig. 13.

The ABSI's springs constants (on the Fig. 13) are

$$\begin{cases} k_{AD} = \frac{\rho_{AD}}{(\sqrt{a^2+b^2})^3}, \\ k_{HA} = \frac{\rho_{HA}}{a^3}, \\ k_{HD} = \frac{\rho_{HD}}{b^3}. \end{cases}$$

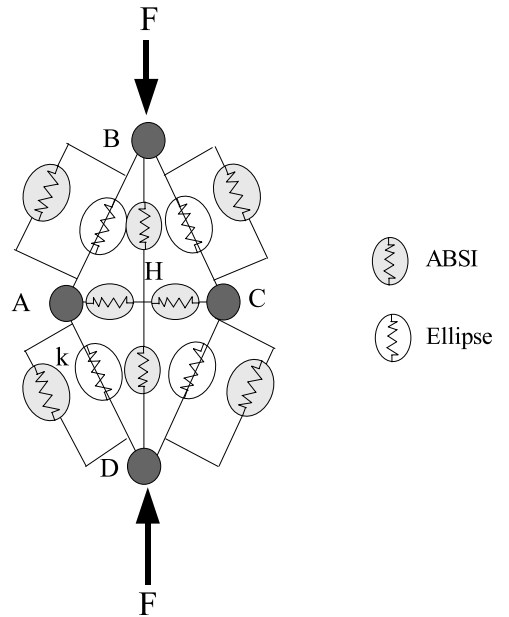And the α angle is equal to $\alpha = \arctan(\frac{b}{a})$.

Fig. 13. Ellipse with elastic material.

3.2.3. Discrete model

The deformation of the discrete model uses MENEB-REA's theory. The strain energy is given by Eq. (18).

$$EPT = \frac{C}{4}(\theta^A - \theta_0^A)^2 + \frac{C}{4}(\theta^C - \theta_0^C)^2 + \frac{C}{4}(\theta^B - \theta_0^B)^2$$
$$+ \frac{C}{4}(\theta^D - \theta_0^D)^2 + \frac{k + k_{AD}}{2}(L_{AB} - L_{AB}^0)^2$$
$$+ \frac{k + k_{AD}}{2}(L_{BC} - L_{BC}^0)^2 + \frac{k + k_{AD}}{2}(L_{CD} - L_{CD}^0)^2$$
$$+ \frac{k + k_{AD}}{2}(L_{DA} - L_{DA}^0)^2 + \frac{k_{HA}}{2}u_C + \frac{k_{HA}}{2}u_A$$
$$+ \frac{k_{HD}}{2}v_D + \frac{k_{HD}}{2}v_B - Fv_D - Fv_B. \tag{18}$$

The parameter C, being a parameter of a mechanical characteristic of the single ellipse, is calculated with Eq. (7) and the ellipse analytical-model.

The displacement of nodes are calculated by a minimization of the potential energy. These calculation are carried out using a MATLAB script.

3.3. Numerical analysis

To validate the discrete model, comparisons with the SAMCEF models are presented below in different configurations. In this part, the materials are given in Table 3. The ellipse studied has a long axis (a), a short axis (b) and a load of $-1000N$.

The linear module ASEF is used to calculate the deformation. All models are meshed with surface mesh. The model is shown in Fig. 14.

Table 3
Material properties

	PEI	Elastic material
Elastic modulus (Pa)	3.1×10^{10}	2.3×10^7
Poisson's ratio	0.36	0.46
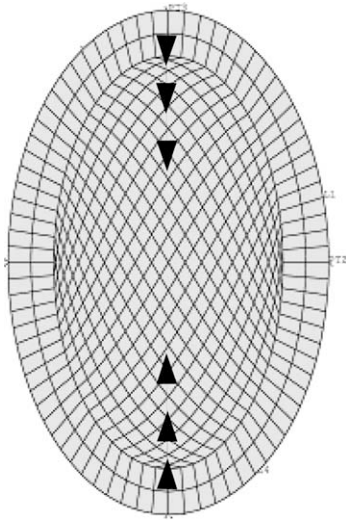
Fig. 14. Finite elements model with elastic material.

Table 4
Displacement results (in mm)

Cases		1	2	3	4	5	6	7	8	9	10
a		8	8	8	8	10	10	10	10	12	12
b		6	8	10	20	6	8	10	20	20	6
H		4	4	4	4	4	4	4	4	4	4
B		4	4	4	4	4	4	4	4	4	4
SAMCEF	u_a	3.63×10^{-2}	5.42×10^{-2}	7.37×10^{-2}	1.72×10^{-1}	4.92×10^{-2}	7.40×10^{-2}	1.01×10^{-1}	2.45×10^{-1}	3.25×10^{-1}	6.34×10^{-2}
	v_b	6.56×10^{-2}	7.39×10^{-2}	8.09×10^{-2}	1.00×10^{-1}	1.05×10^{-1}	1.19×10^{-1}	1.30×10^{-1}	1.59×10^{-1}	2.38×10^{-1}	1.58×10^{-1}
	v_b/u_a	1.81	1.36	1.09	0.58	2.13	1.61	1.28	0.65	0.73	2.49
Ellipse	u_a	4.40×10^{-2}	6.14×10^{-2}	8.12×10^{-2}	2.01×10^{-1}	6.09×10^{-2}	8.52×10^{-2}	1.13×10^{-1}	2.82×10^{-1}	3.72×10^{-1}	7.88×10^{-2}
	v_b	6.92×10^{-2}	7.32×10^{-2}	7.84×10^{-2}	1.04×10^{-1}	1.14×10^{-1}	1.21×10^{-1}	1.28×10^{-1}	1.66×10^{-1}	2.52×10^{-1}	1.73×10^{-1}
	v_b/u_a	1.57	1.19	0.96	0.52	1.87	1.42	1.13	0.60	0.67	2.20

The model has 560 elements and 1921 nodes. The elastic material is merged with the ellipse. The load is applied on the line of nodes (Fig. 14).

3.4. Results and discussion

The MATLAB script is used to calculate the deformation. The displacement results are summarized in Table 4. Figs. 15 and 16 show the evolution of the relative error for u_A and v_B.

Fig. 15 shows the relative error of the displacement u_A. The maximal value of error is 25%. In Fig. 16 the maximal value is 10%.

The discrete model is a good prediction for a ellipse with an elastic material. And this model can be improved with more numbers of springs for the characterization of a single ellipse.
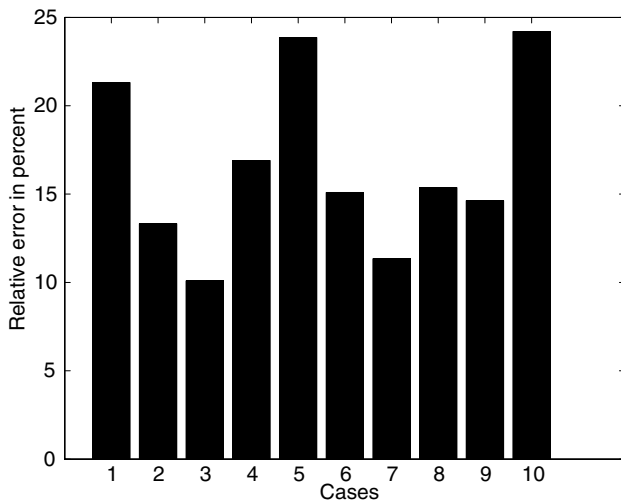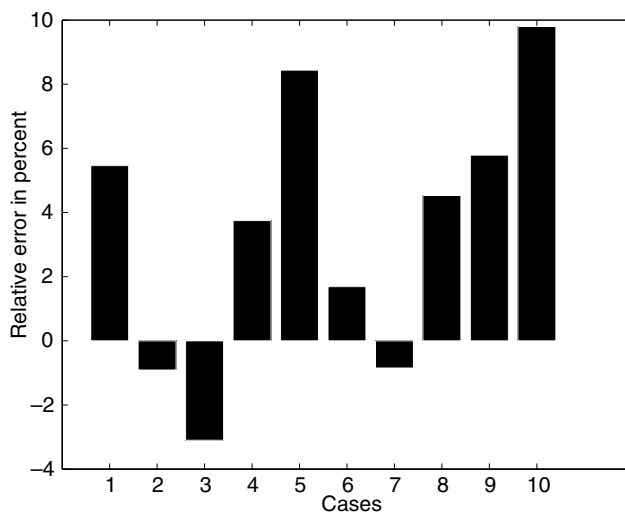

Fig. 15. u_a relative error.

Fig. 16. v_b relative error.

Table 4 also gives the rate of damping. The rate is important when the long axis a is bigger than the short axis b.

4. Conclusion

This work presents the development and the validation of two models. These models are compared with finite element models. The primary conclusions are:

1. The theoretical model for the ellipse has less than 4% of relative error compared to the finite element models.
2. A plate can be modeled by a trellis of beams with ABSI's theory.
3. An ellipse filled with elastic material can be modeled by a discrete model, and gives 25% of maximal relative error.

From this study, it can be concluded that a discrete model can model ellipse deformation. However, an improvement of the discrete model with more than eight springs is considered, and a discrete model of an ellipse trellis is also considered.

This computation clearly shows that such a simple analysis remains useful, as it allows a reliable approach to complex materials, by an energetical method. These kinds of elliptical materials are certain to be used more and more, not only for their static equivalent properties, but also in dynamics. Consequently, the general energetical approach proposed in this paper can be easily extended to dynamic modeling, by addition of kinetic energy, and eventually dissipation power. The distinction between linear and nonlinear rheology is then assumed by quadratic criteria on energies and powers in relation with velocities.

In addition, a similar methodology is suitable to take into account membrane shear stress in such alveoled reinforced materials, and also transverse deflections including plate bending and transverse shear force flows.

References

[1] ABSI E. La théorie des équivalences et son application à l'étude des ouvrages d'art. Annales de l'institut Technique du batiment et des Travaux Publics 1971;153:58–79.

[2] Tse P, Lung C. Large deflection of elastic composite circular springs under uniaxial tension. Int J Non-linear Mech 2000;35:293–307.

[3] Tse P, Reid S, Lau K, Wong W. Large deflection of composite circular springs with axtented flat contact surfaces. Compos Struct 2004;63:253–60.

[4] Tse P, Lau K, Wong W, Reid S. Spring stiffness of composite circular springs with extented flat contact surfaces under unidirectional line loading and surface loading configurations. Compos Struct 2002;55:367–86.

[5] Tse P, Lai T, So C, Chong C. Large deflection of elastic composite circular springs under uniaxial compression. Int J Non-linear Mech 1994;29:781–98.

[6] Ellison J, Ahmadi G, Kehoe M. Passive vibration control of airborne equipment using a circular steel ring. J Sound Vibra 2004;246:1–28.

[7] Huang C, Tseng Y, Nieh K. An analytical solution for in-plane free vibration and stability of loaded elliptic arches. Comput Struct 2003;81:1311–27.

[8] Ford C, Gi L. Uniaxial strength asymmetry in cellular materials. Int J Mech Sci 1998;40:521–31.

[9] S. Laroze, Mécanique des structures, Tomes 1 et 2, EYROLLES, 1988.

[10] Timoshenko S, Goodier J. Théorie de l'élasticité. second ed. Baranger, Paris, France: Librairie Polytechnique CH; 1961.